Preprints.org

Article

Coupling Nanowire Quantum Dots to Optical Waveguides by Microsphere Induced Photonic Nanojet

Symeon I Tsintzos , Konstantinos Tsimvrakidis , James C Gates , Ali W Elshaari , Peter G.R. Smith , Val Zwiller , Christos Riziotis *

Article

Coupling Nanowire Quantum Dots to Optical Waveguides by Microsphere Induced Photonic Nanojet

Symeon I. Tsintzos [1,†], Konstantinos Tsimvrakidis [1], James C. Gates [2], Ali W. Elshaari [3], Peter G.R. Smith [2], Val Zwiller [3] and Christos Riziotis [1,4,*]

[1] Theoretical & Physical Chemistry Institute, National Hellenic Research Foundation, 11635 Athens, Greece
[2] Optoelectronics Research Centre, University of Southampton, SO17 1BJ Southampton, United Kingdom
[3] Department of Applied Physics, Royal Institute of Technology (KTH), 106 91 Stockholm, Sweden
[4] Institute for Advanced Modelling and Simulation, University of Nicosia, CY-2417 Nicosia, Cyprus
[*] Correspondence: author (C. Riziotis): Tel: (+30) 2107273887, e-mail: Riziotis@eie.gr
[†] Present address: QUBITECH Quantum Technologies, 15231 Chalandri, Athens, Greece.

Abstract: Silica on Silicon is a major optical integration platform, while the emergent class of integrated Laser written circuits' platform offers additionally high customizability, and flexibility for rapid prototyping. However, the inherent waveguides' low core/cladding refractive index contrast characteristic compared to other photonic platforms in silicon or silicon nitride, sets serious limitations for on-chip efficient coupling with single photon emitters, like semiconductor nanowires with quantum dots limiting the applications in quantum computing. A new light coupling scheme proposed here overcomes this limitation providing means for light coupling >50%. The scheme is based on the incorporation of an optical microsphere between the nanowire and the waveguide, properly optimized and arranged in terms of: size, refractive index, distance of microsphere between nanowire and waveguide. Upon suitable design of the optical arrangement, the photonic nanojet emitted by the illuminated microsphere excites efficiently the guided eigenmodes of the input channel waveguide, thus launching light with high coupling efficiency. The method is tolerant in displacements, misalignments, and imperfections and is fabricationally feasible by current state of the art techniques. The proposed method enables the on-chip multiple single photon emitters' integration thus allowing the development of highly customizable and scalable quantum photonic integrated circuits for quantum computing.

Keywords: waveguides; nanowires; quantum dots; quantum emitters; microspheres; photonic nanojet; silica; quantum circuits; quantum computing

1. Introduction

Photonic integrated circuits (PICs) are nowadays considered as a versatile platform for quantum technology applications due to their scalability, robustness, and miniaturization characteristics [1–3]. By exploiting fabrication advances in the mature optical integrated circuits for telecommunications field, on-chip scale manipulation of quantum light states [4–10] in integrated quantum photonics systems increases dramatically the component density, loss and phase stability compared to other bulkier optical approaches. These implementations a have allowed initial demonstrations of the operating principle of quantum simulators [11,12], quantum machine learning [13], fundamental tests of quantum mechanics [14], and a new generation of quantum optical processors [15–17]. However, to develop a fully operational standalone quantum PIC, issues in photon generation, light manipulation and detection, all taking place on the same chip, have to be overcome. The full integration of a photonic system remains a pending challenge for the photonic community because of the specialized material requirements for each distinct component. For this reason, a number of emitters [18–20] and photonic platforms [21] have been proposed, combining individual material components toward the development of complete hybrid photonic systems [1,21].

Silica-on-silicon [3] is an ideal candidate for waveguide quantum circuits since it couples efficiently to single mode optical fibers, and exhibits low waveguide propagation losses. In addition, silica is transparent to a wide range of wavelengths enabling the integration of various quantum single photon emitters, extending from the UV to IR optical region. Recent demonstrations of on-chip single-photon detectors [22], thermo-optical phase shifters for reconfigurable circuits [23], or on-chip implementation of quantum gates [10,24], set the scene for such a platform toward the realization of a fully integrated quantum photonic system.

Although these pioneering achievements illustrate the silica based platform as a remarkable platform for integrated quantum applications, the on-chip incorporation of a single photon emitter remains a challenging task, since at present the most common mechanism to generate single photons is by a spontaneous parametric down conversion of light externally [7] or on-chip [25] which is highly inefficient and probabilistic in nature. This also limits the scalability by not providing means of on chip embedded single photon sources. A most promising solution to this problem, among other single photon sources, is the use of quantum dots (QDs) which are suitable for on demand single and entangled photons generation, exhibit indistinguishability, narrow emission linewidth and emission tunability, upon being electrically pumped [26–28]. In addition, by embedding the QD in a photonic nanowire (NW) during the growth process, directional and Gaussian profile emission is observed, since the QD spontaneous emission couples to the nanowire's fundamental mode, making the nanowire quantum dot (NWQD) system [29–31] suitable for coupling to internal or external waveguides. Up to now, efficient NWQD coupling has been achieved in silicon nitride [32–34] and Si platforms [35,36] due to the compatibility of the corresponding channel waveguide dimensions and refractive indices with NWQD structures.

Nanowires or NWQD integration in silica or silica on silicon optical waveguides has not been possible until now due to major incompatibility issues between the material, optical and waveguiding properties of semiconductor nanowires and silica based waveguides. Furthermore, an important method of fabrication silica based optical circuits is by Direct Laser Writing (DLW), by Excimer Lasers [37], femtosecond Laser, [38–40] Ultraviolet Laser [7,41]. The laser induced refractive index modification defines channel optical waveguides, thus allowing the rapid customization and fabrication of complex highly functional optical circuits. However, this DLW method creates optical waveguides of low refractive index change (typical refractive index increase ~$5*10^{-3}$) of low or medium optical confinement and typical waveguide mode diameter larger than 5 μm, setting additional incompatibility and restrictive issues for NWQD coupling to such Laser written waveguides. Similar waveguiding characteristics are also apparent in buried in-diffused waveguides fabricated by other chemical and physical techniques different to Laser writing. Furthermore the refractive index contrast between overcladding and core waveguide is still low also to silica based waveguides and circuits fabricated with high cost lithographic techniques [3] such as Reactive Ion Etching. In such low refractive index contrast optical waveguides the modal characteristics are highly different in terms of numerical aperture, waveguide's modal size, refractive index, and it was shown recently [42,43] that these factors can limit the coupling to a level <5% which is inadequate for practical applications. It is clear that new coupling approaches are needed to overcome the problem and enable the incorporation of single photon sources in silica based waveguides.

In this work, we propose for the first time a systematic study on a novel approach for coupling a NWQD to a low refractive index contrast single-mode buried silica waveguide. We demonstrate this coupling scheme, by providing the design, and the performance evaluation, together with a performance limitations and tolerances studies, for the representative and most challenging case of coupling a typical semiconductor NWQD to a typical Laser written channel waveguide in silica. The coupling scheme is based on the photonic nanojet action of a suitably designed microsphere [44] that is placed between the nanowire and the channel waveguide and excites efficiently the waveguide through the nanojet's optical field. The approach of nanojet's assisted light coupling could be of generic application and could be used in various light coupling problems in photonics, however in this paper is focused on the specific case between nanowire and channel optical waveguides which attracts considerable interest in quantum computing applications.

2. NWQD Coupling Limitations with Waveguides

This section provides the background problem formulation, by employing numerical simulations, on the coupling of a typical III-V semiconductor NWQD photon emitter to a Laser written single mode silica waveguide (WG). The major obstacles preventing the efficient coupling of these two photonic components arise from their very different sizes and optical properties. The characteristics of the silica platform, is that the silica refractive index is low (1.452), while the Laser induced refractive index modification, which defines the waveguide core, lies in the range of 10^{-3} - $5 \cdot 10^{-3}$. This low refractive index contrast of core/cladding poses limitations to the waveguide's diameter, which is typically 3-5 μm, to ensure a single mode operation. On the other side, the diameter of a III-V semiconductor NWQD is much smaller at 200-400 nm diameter and when tapered its end diameter can be down to 80-150 nm, while its refractive index value is as high as 3.4. The cross-sectional area of a SiO$_2$ waveguide, assuming a 3 μm diameter, is almost 600 times larger than that of the tapered NWQD tip, requiring additional components to adjust the mode field diameter accordingly.

As an introduction to the aforementioned problem an initial study on the coupling limitations is provided. As a physical simulation scenario, it is considered an arrangement of a nanowire quantum dot emitter and a buried channel waveguide in a homogeneous medium, as shown in Figure 1 (a). The single photon emitter is a typical [45] III-V Indium Arsenide Phosphide InAsP QD, which is embodied in an Indium Phosphide InP NW during the growth process. The designed NW is 4 μm long with a diameter of 200 nm while the taper diameter at the end of the NW is 109nm corresponding to a taper angle of 2°. The location of the QD is 200 nm from the NW's base. This specific nanowire geometry is designed and tuned for 880 nm operating wavelength. The considered NWQD was a typical and characteristic option, with high availability for future experimental validation, while this choice does not restrict the applicability of the results in other nanowires of similar or larger dimensions, various tapering shapes, and at different operating wavelength bands, as discussed also in [43].

We also consider the simplified case of a uniform cylindrical optical waveguide with a circular cross-section embedded in the homogeneous medium of lower refractive index. Such a channel waveguide refers to a typical Laser written or in general of a buried waveguide. To ensure the single mode operation for the photonic channel at the 880 nm QD's emission wavelength, the refractive index contrast, $\Delta = (n^2_{core} - n^2_{cladding})/2n^2_{core}$, between the core and the cladding has to be adjusted properly. For a silica medium (n = 1.452) as the cladding in our system, we assume a core refractive index Laser modification of $\Delta n = 5 \cdot 10^{-3}$, for a waveguide of 3 μm diameter. A refractive index difference of this value ensures a single TE/TM mode operation and provides moderate confinement along the waveguide's cross-section plane, thus striking a balance between light guidance and minimizing the effects of fabrication or modeling imperfections.
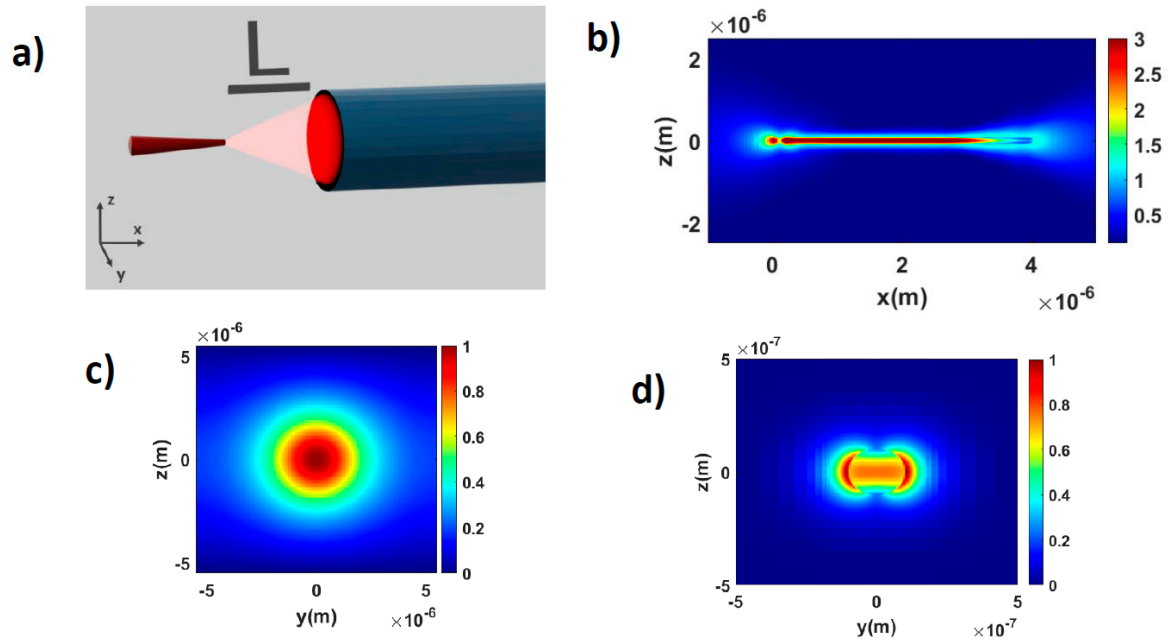
Figure 1. (a) Illustration of the photonic structure under investigation. (b) NWQD electric field distribution along the XZ plane. Cross-sectional electric field intensity distribution of the TE supported mode for the (c) waveguide and (d) NWQD respectively.

Initially, we examine the geometry shown in Figure 1(a), assuming that both NWQD and the WG are aligned in an inline arrangement and L is their relative distance. To facilitate our calculations, we regard that the whole structure (NWQD and WG) is surrounded by homogeneous SiO_2 material. In general, to achieve efficient coupling between the two distinct waveguides of different dimensions, one has to carefully design the two structures in order to obtain i) similar effective refractive indices and ii) maximum overlap integral between the fields of the two interacting modes. In our case, the supported TE/TM fundamental modes for both the NWQD and the SiO2 waveguide are shown in Figure 1 (c) and (d).

The calculation of the light coupling is performed by 3-dimensional (3D) Finite Difference Time Domain (FDTD) numerical simulations (Lumerical Inc, USA). The model takes into account the overlap between a QD TE electric dipole moment, embedded in the nanowire, and the waveguide's fundamental TE mode to accurately compute the coupling. In Figure 2(a), the evaluated coupling values are shown as a function of the relative distance L for a TE dipole NWQD emission. The corresponding distribution of the TE electric field along the XZ plane is shown in Figure 2(b). From the electric field distribution at the XZ plane, we observe that most of the NWQD emitted light dissipates out of the waveguide and only a small portion of that couples to the waveguide's fundamental TE mode, dramatically reducing the coupling value to ~4%, while for higher coupling above 10% a Δn much higher than 10^{-2} is required [43], which is beyond the current fabrication capabilities in silica platform. This finding confirms that the major hurdle behind the inefficient coupling between the NWQD and the WG is the large NA difference of the two photonic blocks, due to the low refractive index contrast of the channel waveguide.
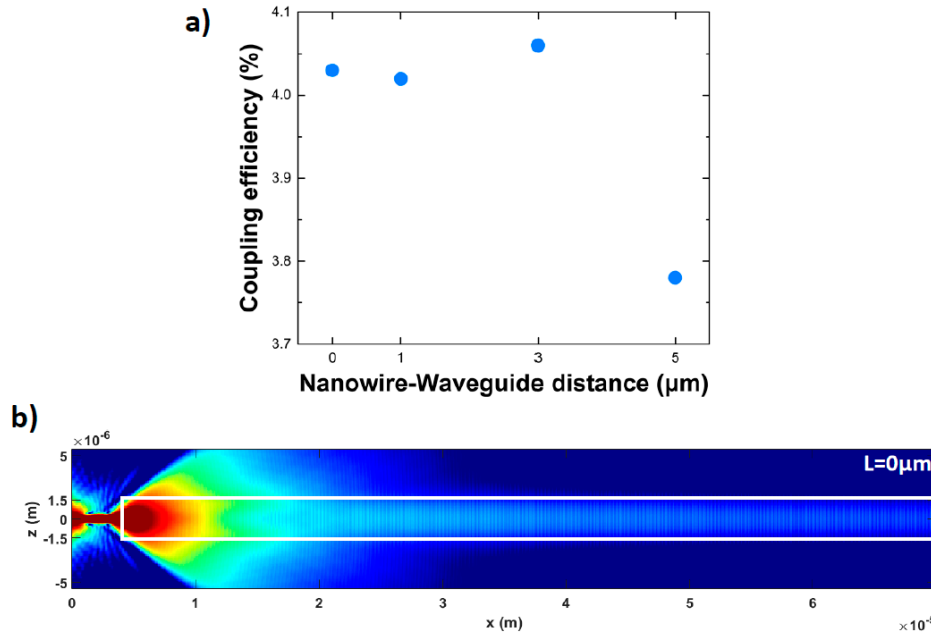
Figure 2. a) Extracted NQD-WG coupling values assuming TE dipole emission. b) Electric field distribution along the XZ propagation plane for the indicative case of the relative NW-waveguide distance L=0μm, and for propagation distance 70μm. The graphs are presented in logarithmic scale for clarity.

3. NWQD -Waveguide Coupling Scheme

To overcome the aforementioned inherent light coupling limitation and negate the high NA difference, the use of an optical dielectric microsphere as an intermediate element placed between the NWQD and the WG is proposed for the first time. It is demonstrated in the paper that in the mesoscale microspheres regime proposed here the induced photonic nanojet [46–48] succeeds to eject the light, illuminated by the NWQD, into the receiving channel waveguide. Figure 3 (a) illustrates the investigated photonic system with the addition of the microsphere represented in a generic case with a cylindrically shaped waveguide embedded in a uniform lower refractive index medium. In the same Figure 3a it is represented also schematically a more realistic implementation of microsphere's arrangement between a buried orthogonal channel waveguide and a suitably aligned nanowire. For clarity of the results' presentation   and the demonstration of the operating principle we are restricting our study here in the ideal case of cylindrical wave guide. It has been confirmed by our studies that similar behavior and coupling performance can be achieved for the buried waveguide case, however as this geometry includes various additional parameters for optimization it will be reported in a future study.

More specifically, in this generic arrangement of the proposed coupling method, we consider that the separation between the end tip of NWQD and the adjacent surface of the microsphere is L, while the separation between the surface of the microsphere adjacent to the end of the waveguide and the waveguide is D. For a specified optical nanowire and a specified channel optical waveguide, the microsphere can be appropriately designed, and selected in terms of characteristics, such as: i) refractive index, ii) dimension (diameter), and arranged properly in terms of: iii) geometrical separation between the nanowire and the microsphere, iv) geometrical separation between the microsphere and the waveguide, in order to achieve the maximum light coupling from the nanowire to the optical waveguide. In the generic case the microsphere could be a proper dielectric microelement such as a cylinder, or a half cylinder, or half sphere, however for simplicity the study here was concentrated only   to microspheres which could be readily available.

For a properly designed arrangement, the photonic nanojet emitted by the microsphere induces proper launching conditions in the vicinity of the adjacent waveguide leading to proper excitation of

the waveguide's supported guided optical modes resulting in efficient coupling of nanowire's emitted light to waveguide's guided light at the fundamental or other higher-ordered modes.

It is stressed here that the proposed coupling system and method is based on this excitation of waveguides by the induced photonic nanojet. The microsphere does not act as a focusing ball lens that concentrates light into a single point, as it happens in other focusing techniques when using focusing balls of dimensions much greater of $30*\lambda$ determined my geometrical optics principles with a well defined optical focal point.

The microspheres considered in this study have a diameter in the range of 2-12 μm. In this scale where the size of the microsphere is comparable to the wavelength of the incident light, their interaction with light cannot be described geometrical optics approach or by Rayleigh scattering formalism. However, a full description of light interaction with spherical particles of arbitrary size can by provided by Mie theory and associated following formalisms as in [48], where it has been shown that the field enhancement by dielectric mesoscale spheres (with radius R spanning from 1-30 λ), leads to a jet shaped beam, usually called photonic nanojet. The spatial characteristics of a photonic nanojet can be easily modulated [46–48] as they depend on the microsphere size, the refractive index ratio between the microsphere, the surrounding material and the wavelength of the light. Photonic nanojets are essentially scattered beams of light with a high-intensity main lobe, a weak sub-diffracting waist and a very low divergence angle.

Until today, in the current state of the art, it was not never considered or applied in practice the employment of microsphere for the generation of a photonic nanojet in order to launch and couple light in a waveguide, or even more specifically to launch light in a waveguide when illuminated by a nanowire or by a nanowire with a quantum dot acting as single photon source. Photonic nanojets were studied and demonstrated only in the following cases and applications: Enhanced Raman spectroscopy, photolithography, nanoparticle detection and manipulation, enhanced optical absorption in photovoltaics and photodiodes, Laser materials processing and dry Laser cleaning, Fluorescence sensing, high -density optical data storage [46], but not for coupling light to waveguides as described and demonstrated in this work.

3.1. Simulation of Photonic Nanojet Action

To highlight the role of the microsphere's characteristics in the nanojet's formation, such as the refractive index and radius, we initially simulate by FDTD a standalone microsphere illuminated by the NWQD assuming no presence of a waveguide in the vicinity of the microsphere. Photonic nanojets simulation can be efficiently and reliably performed by Finite Element Method (FEM) [49] or by FDTD as is used here with an adequately dense computational grid [47], leading to very close agreement with analytical derivations based on Bromwich scalar potential formulation [48]. Here, it was followed an FDTD simulation approach in order to include and study the light propagation in the entire system of nanowire, microsphere and channel waveguide. To formulate the problem, we consider microspheres with refractive index spanning from 1.6 to 2.5, simulating different microsphere materials, such as Polystyrene (n=1.6), Alumina (Al_2O_3, n_{Al}=1.76), Barium Titanate (n_{Ba}=1.9, 2.2) or Titania (n_{Ti}=2.5). Figure 3(b), (c), summarize the results obtained from FDTD simulations for different microsphere refractive indices and diameters at NWQD-microsphere distance L = 0 μm. Figure 3 (c) show the nanojet formation for NWQD-microsphere distance equal to L= 0, 1, and 3 μm with microsphere refractive index 1.9 and diameter set to 6 μm. Background refractive index is n=1.452.
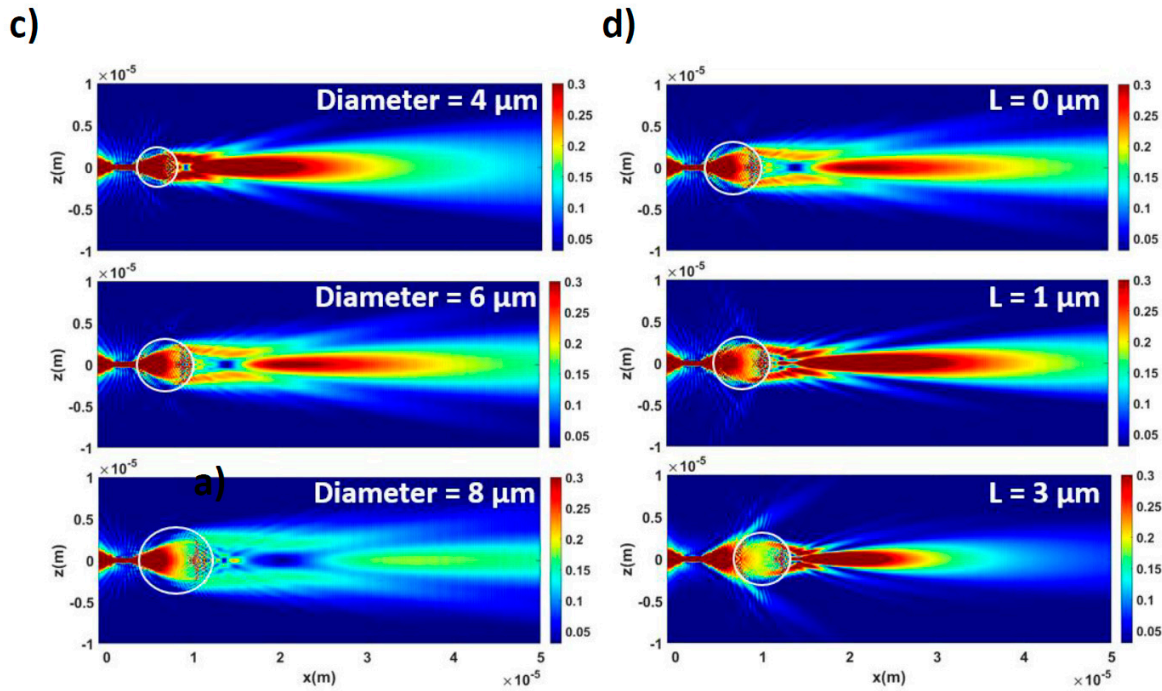
a)

b)
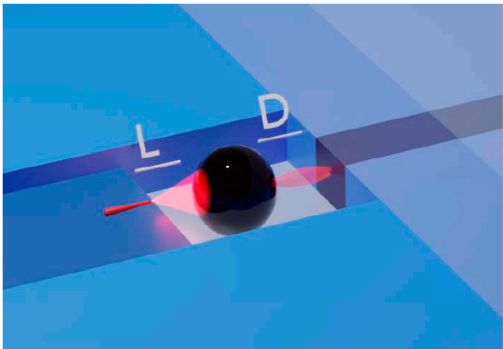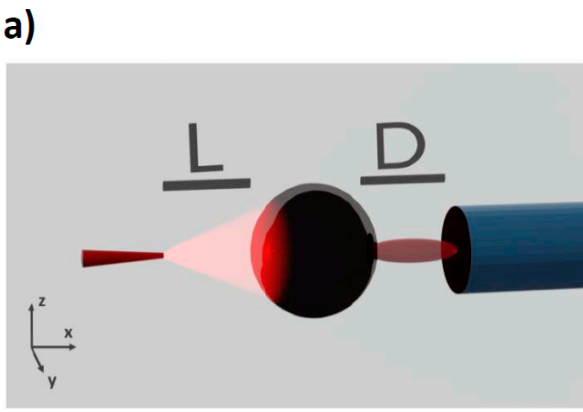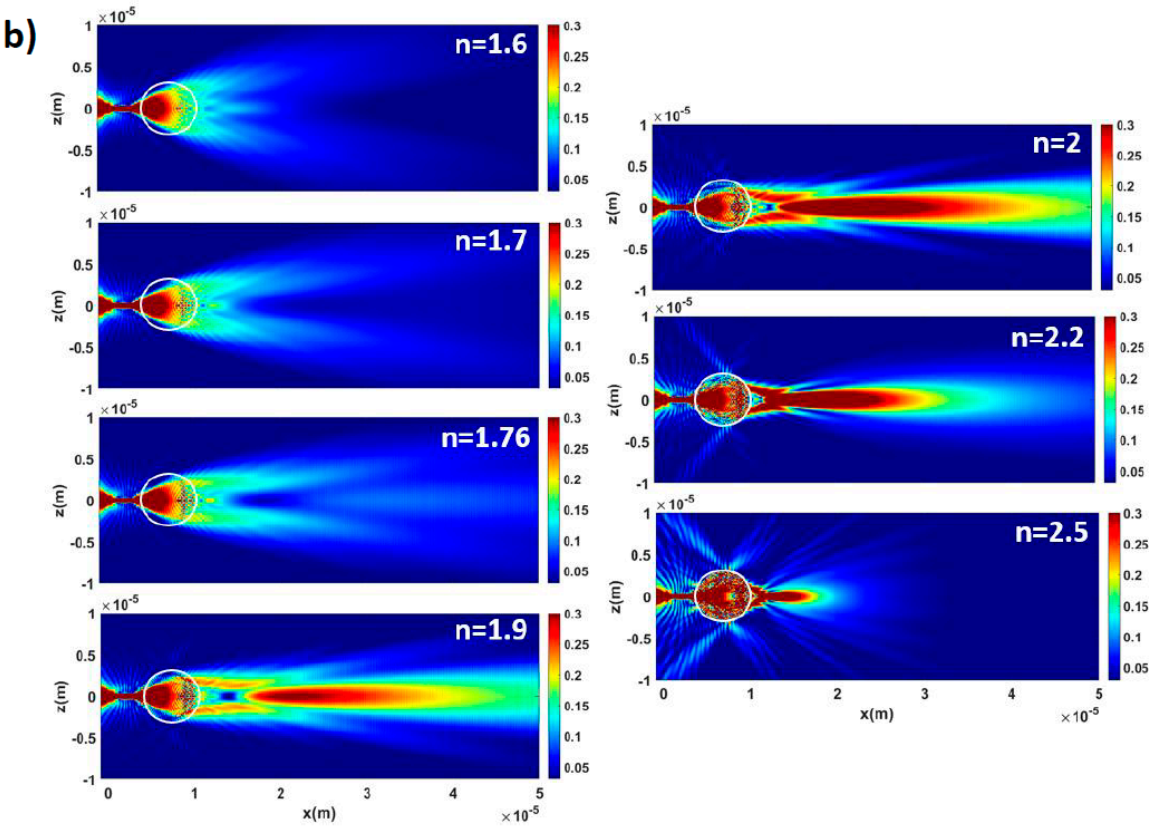
Figure 3. a) Artistic illustration of the photonic structure with the microsphere and the photonic nanojet. b) XZ plane TE electric field distribution and photonic nanojet formation for different refractive index microspheres with diameter 6 μm at L=0 μm c) Formation of photonic nanojet for three distinct microsphere (n = 1.9) diameters 4μm, 6μm and 8μm at L = 0 μm. d) Photonic nanojet formation for NQD-microsphere distance L = 0, 1, 3 μm by a 6 μm diameter and n=1.9 microsphere. Background refractive index is n = 1.452.

In Figure 3 (b), where the microsphere's diameter is kept constant and equal to 6 μm, we observe that as the refractive index ratio of the microsphere to the background (n=1.452) increases, the formation of the photonic nanojet occurs closer to the shadow side surface or even inside the microsphere for high enough refractive index (e.g., 2.5), its elongation along the propagation axis reduces, the peak intensity increases and the FWHM becomes narrower. The results presented here are in agreement with existing findings [47]. In Figure 3 (c), the effect of the increasing diameter of a microsphere with n=1.9 is examined and it is observed that the nanojet is formed effectively for lower diameter microspheres. Additionally, in Figure 3 (d) the distance between the nanowire and the microsphere is altered for the case of a microsphere with diameter of 6μm and refractive index of 1.9. As the nanowire-microsphere distance increases from 0μm to 1μm and 3μm we notice that the nanojet increases in intensity with shorter length along the propagation axis and moves closer to the microsphere's shadow side. This observation is quite comprehensible as in this specific microsphere with a relatively high refractive index (n = 1.9), when the distance from the source is increased, the microsphere collects the impinged light in a bigger angle and redirects it closer to the shadow surface forming a more compact and of higher intensity photonic nanojet. In general, we notice that the addition of the microsphere modifies the spatial characteristics of the emitted NWQD light, since the produced photonic jet is considerably more directional in respect to the Gaussian emission of the NWQD.

3.2. Coupling to Waveguide through the Nanojet Excitation

To evaluate the role of the microsphere in the NWQD-WG coupling, we conducted extensive FDTD calculations in the full photonic structure as depicted in the Figure 3(a). The parameters examined are the microsphere's diameter and refractive index. Furthermore, to relate our study to a

more realistic experimental implementation of a photonic circuit we take into account the effect of the relative distance L between the NWQD and the microsphere on the coupling calculation.

The coupling efficiency values are extracted for microspheres of different refractive index value (n = 1.6-2.5) and are plotted in Figure 4 as a function of the radius and the relative distance L.   It is clearly demonstrated that the incorporation of a microsphere appears to significantly improve the NWQD-WG coupling by selecting the appropriate microsphere characteristics and the relative distance L. More specifically, TE mode coupling values as high as 40%-45% can be achieved with precise control of the relative distance L in the case of the n = 1.76, n = 1.9 and n = 2 microspheres while for microspheres with refractive index lower than 1.7 or higher the 2.0 the coupling is drastically decreased. Noteworthy is the fact that the coupling efficiency is very sensitive to the relative distance between the nanowire and the microsphere. Small deviations from the optimum design are possible to gradually downgrade the coupling efficiency. The coupling efficiency values extracted with the aid of a microsphere are more than an order of magnitude greater than those obtained without the microsphere by just butt-coupling the nanowire to the waveguide. The Supplementary Material section provides visual details of the coupling mechanism, for indicative cases of coupling for the configurations illustrated in Figure 4. Coupling is demonstrated in Figures S1 (a) -S7 (a) for the selected distance L that achieves maximum coupling value for a specific diameter, whiles graphs S1 (b) -S7 (b) provide a detailed view for the maximum coupling case.
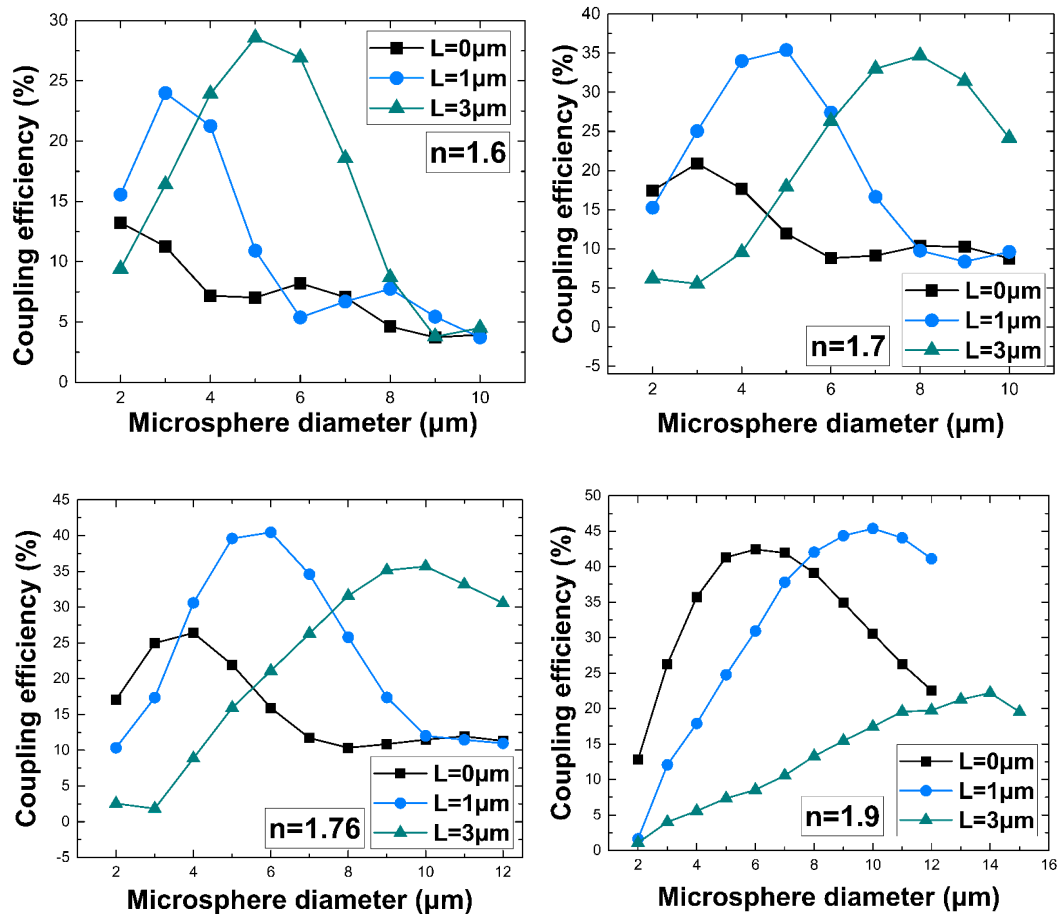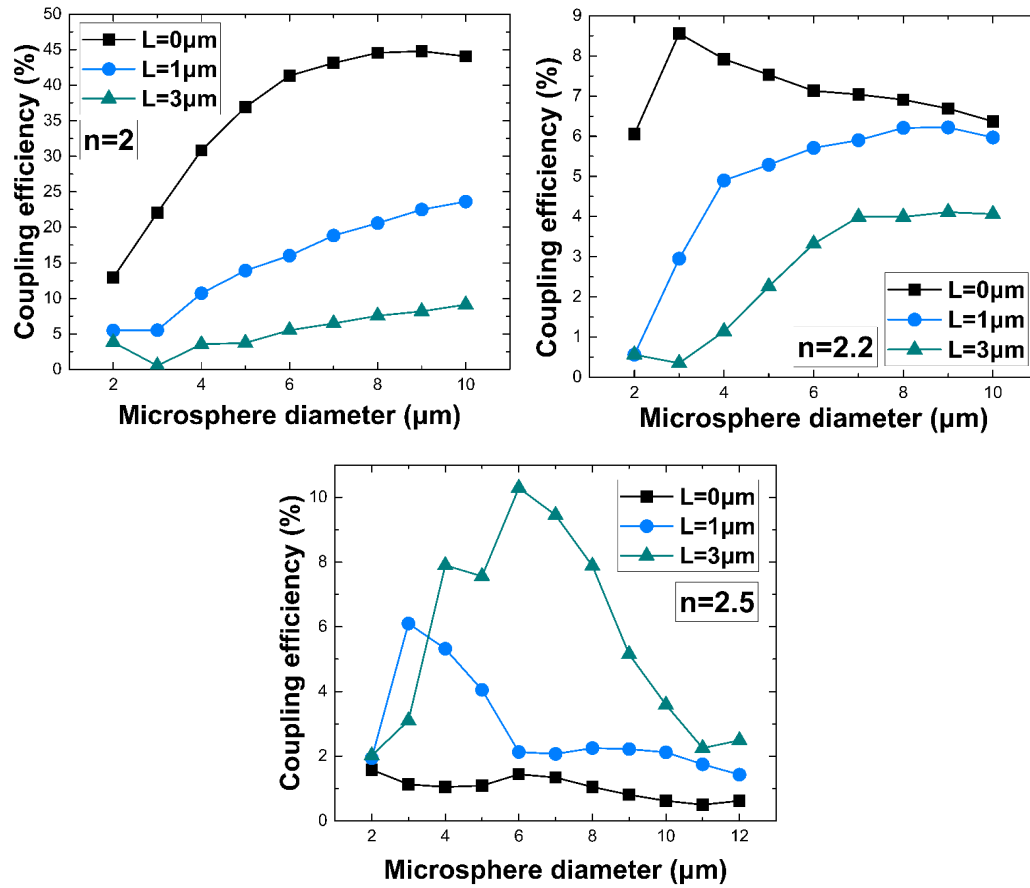
Figure 4. Coupling values over NWQD-microsphere relative distance L = 0, 1 and 3 μm for n = 1.6, 1.7, 1.76, 1.9, 2, 2.2 and 2.5 microspheres with diameter ranging from 2 μm to 15 μm.

To provide an intuitive view of the coupling mechanism, Figure 5 presents a selection of the cases considered in Figure 4 with the parameters selected for providing the highest coupling. Depending on the considered parameters it is shown how the nanojets is injected in the adjacent waveguide transforming its energy to the supported fundamental guided mode of the channel waveguide.   In Figure 4 is clear for a few cases of strong coupling for n= 1.7, 1.76, and 1.9, the existence of two distinct peaks with comparable maximum coupling corresponding to different L. As can be observed from Fig. 3 (c), (d) the interplay between diameter and distance L can provide conditions for comparable efficient coupling but with different ways by directing the light in different positions along the waveguide, as clearly seen also in Figure 5. For clarity the different ways of coupling are demonstrated comparatively in the Supplementary Material section in Fig. S3 (b) and (c), and Figure S4 (b) and (c) for microspheres with refractive index n= 1.76 and 1.9 respectively.
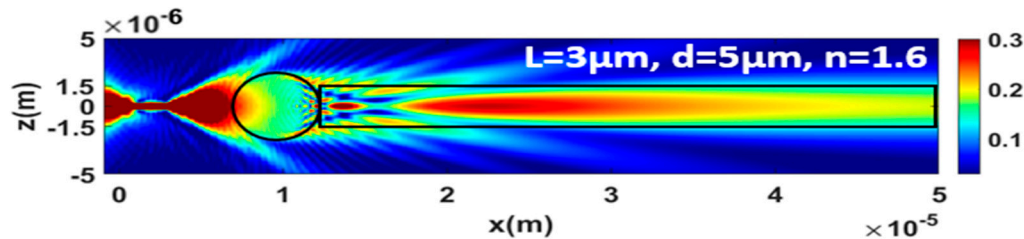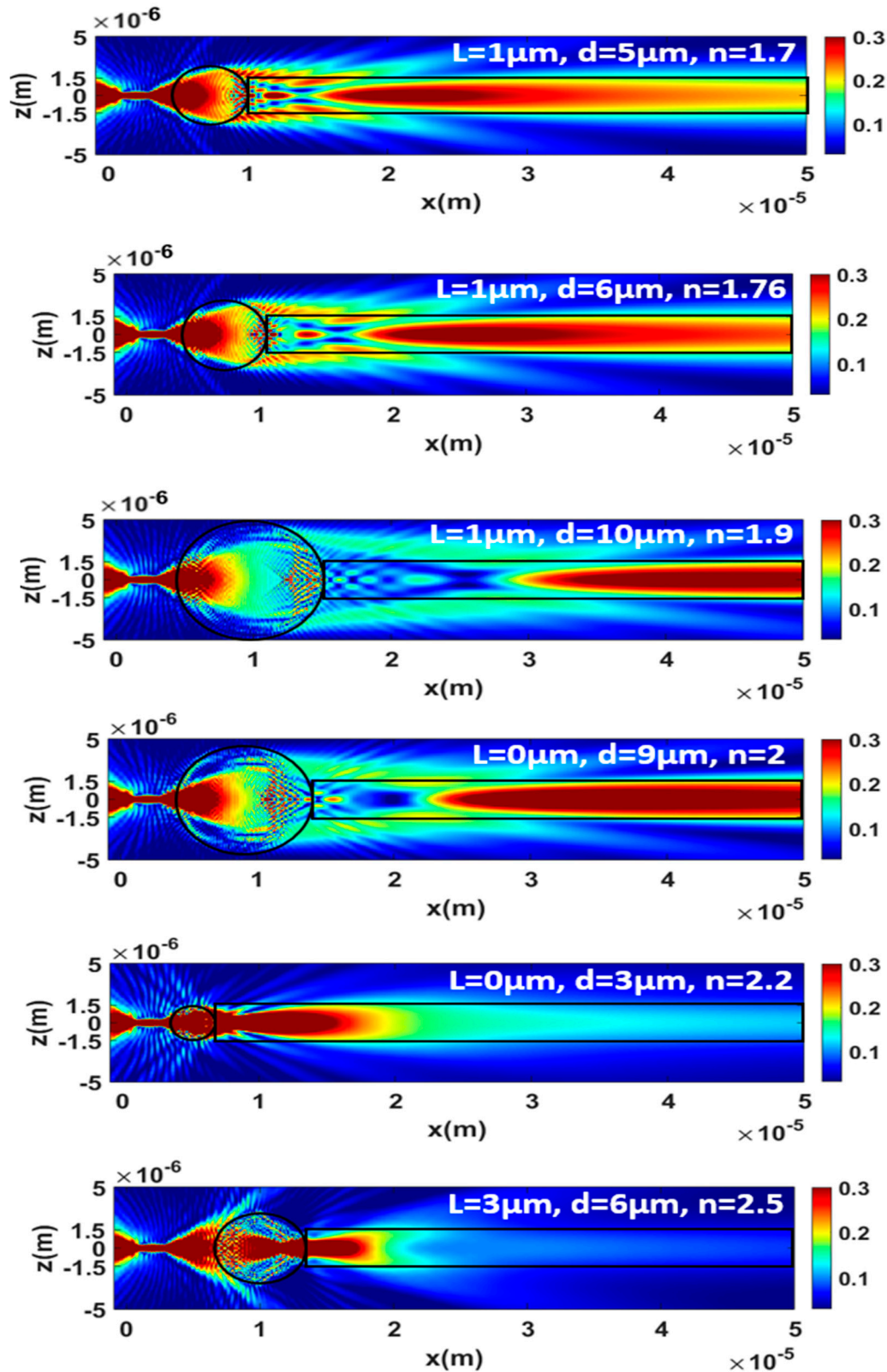
Figure 5. Electric field propagation along the propagation axis for the most efficient case of each microsphere refractive index. L refers to the NWQD-microsphere distance, d is the microsphere diameter and, n is the refractive index of the microsphere.

In order to demonstrate clearly the reliable steady state condition of coupling of the nanojets into the waveguide' supported modes it is provided in Figure 6 the coupling mechanism for the representative case of a highly efficient coupling through a 6 μm diameter, n = 1.9 microsphere at L = 0 μm and over 70μm and 250 μm of waveguide propagation. In the case of 70 μm is can be seen

the details of nanojet formation in presence of the waveguide, while in the 250 µm it is demonstrated the smooth steady state propagation of the supported propagated mode.
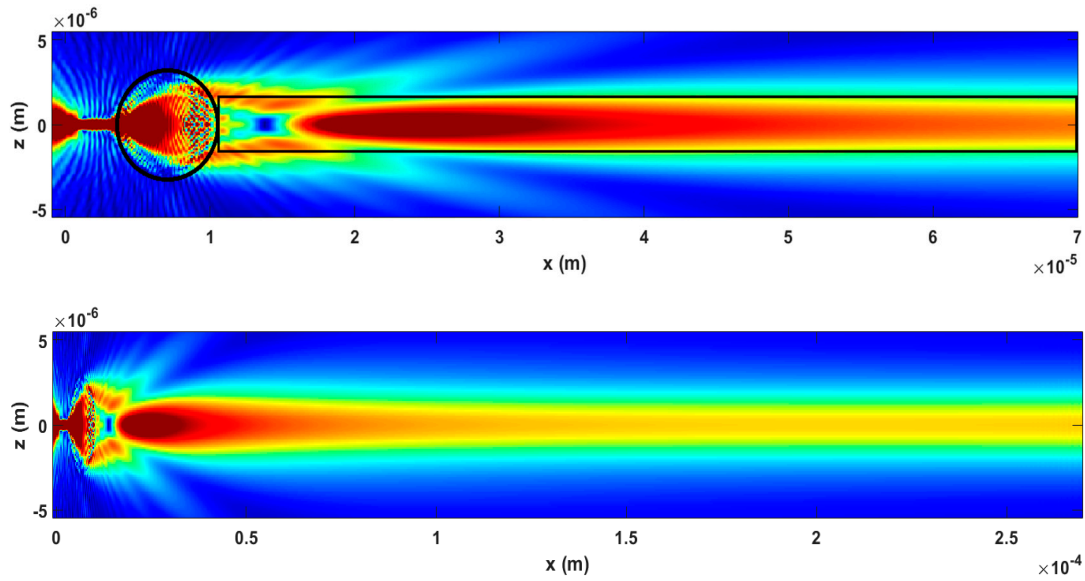

Figure 6. Cross sectional TE electric field distribution along a long-range waveguide through a 6 µm diameter n = 1.9 microsphere set at distance L = 0 µm from the nanowire, for propagation distances of 70 µm (up) and 250 µm (down).
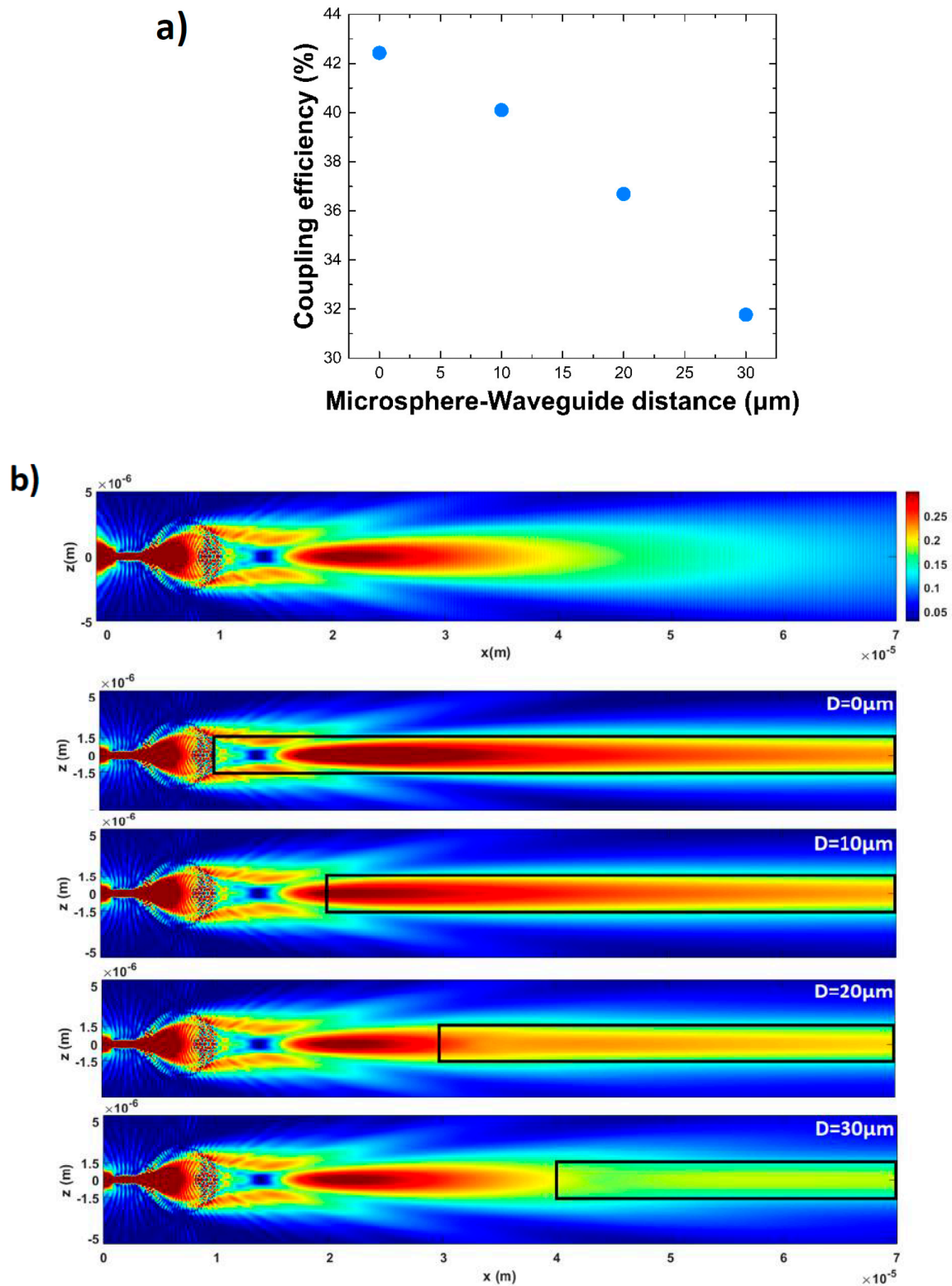
4. Design Tolerances in the Coupling Scheme

Additionally, other secondary parameters are also affecting the coupling efficiency in the proposed method and are taken into account for the theoretical determination of the maximum design coupling. These parameters determine the tolerances of the design and are: i) the effect of distance D between the microsphere and the waveguide, ii) the angle of axis of the NWQD to the central axis of the microsphere that is aligned to the axis of the waveguide inducing a misalignment, iii) the degree of sphericity of the microsphere, iv) the lateral (Y / Z- direction) displacement of the NWQD, and v) the design operating wavelength. It should be noted that despite the fact that the distance D is a key parameter in the optimal arrangement of the proposed coupling scheme (as discussed above)   due to the fact that it   affects less drastically the coupling performance is considered here in the tolerances   section for clarity of presentation reasons.

4.1. Effect of Distance Microsphere - Waveguide

Firstly, we examine the case where the microsphere and the waveguide are no longer in contact, but there is a gap D between them, as shown earlier in Figure 3 (a).

In this section we consider a microsphere with diameter 6 µm and refractive index 1.9 with the distance L between the nanowire and the microsphere set to 0 µm, while the distance D between the microsphere and the waveguide is increased from 0 µm to 10 µm, 20 µm and 30 µm. The corresponding coupling efficiency values versus the gap distance D is shown in Figure 7 (a). Figure 7 (b) presents from top to down the generated photonic nanojets itself (neglecting the presence of the waveguide) followed by the electric field distribution along the propagation axis as the waveguide is moved further away from the microsphere, from 0 to 30 µm. While obtaining a coupling value of over 42% when the microsphere and the waveguide are in touch, when their interspace increases by 10 µm the coupling efficiency appears to drop down only by 2%. By further increasing this gap, the coupling efficiency value keeps decreasing, achieving a value of 37% for a 20 µm gap and about 32% for a 30 µm gap. Comparing the electric field distributions to the case where the nanojet is formed in the medium with no waveguide present we observe the additional confinement of the nanojets inside the waveguide boundaries forcing the excitation of the guided modes.

Figure 7. a) Coupling efficiency versus distance D. b) presents from top to down the generated photonic nanojet (neglecting the presence of the waveguide) followed by the electric field distribution along the propagation axis as the waveguide is moved further away from the microsphere, axis for distance D=0, 10, 20 and 30 μm. The microsphere refractive index is n = 1.9 and its diameter is set to 6 μm.

4.2. Effect of NWQD Tilt Angle

The accurate placement of the NWQD and its alignment with the rest of the photonic blocks is typically performed by accurate transfer techniques, e.g., by employing micro/nano manipulators [34,35]. However, the effect of any tilt misalignments due to an induced tilt of angle φ related to the central axis of a microsphere is also considered. To get a better view on the aforementioned misalignment effect on the coupling efficiency, we performed numerical simulations rotating the NWQD with an angle φ in respect to the nominal propagation axis, as shown in Figure 8.
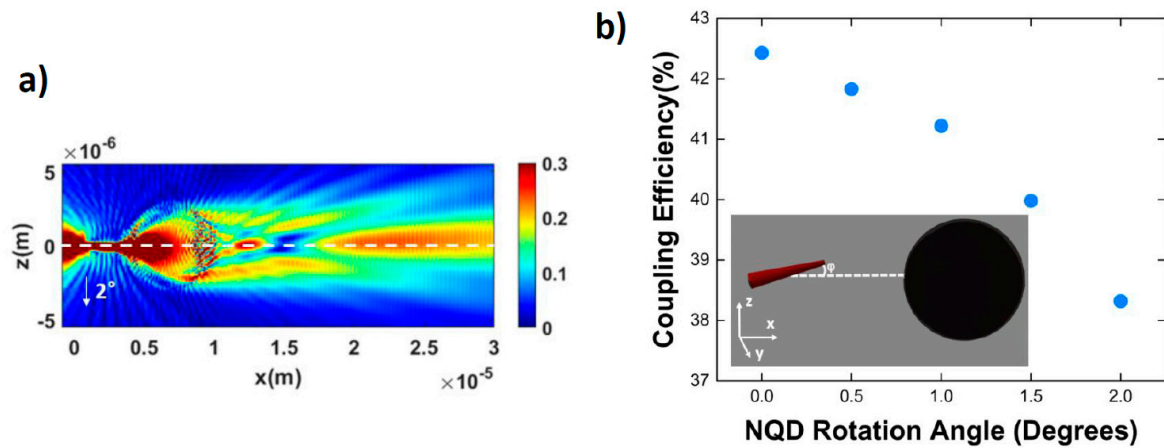

Figure 8. a) Photonic nanojet formed through a 6 μm sphere with the NWQD tilted at 2° away from the center of the microsphere in the Z- direction. b) NWQD-WG coupling values as a function of the rotating angle φ. Inset image illustrates the rotating angle scheme.

In Figure 8 (b), the NWQD-WG coupling is presented, varying the angle to 2°. To carry out these simulations, an arrangement with L = 0 μm and with a microsphere with a 6 μm radius and refractive index n = 1.9 was considered. Despite the rotating angle misalignment between the NWQD and the microsphere, the coupling remains high enough, reduced only by 4% for a maximum rotating angle of 2°, exhibiting the robustness of the system under experimental misalignment issues. State of the art micromanipulation techniques can provide very accurate control of positioning eliminating tilts to angles below 1 degree, and therefore the proposed method is relatively robust to such tilts.

4.3. Effect of NQD Lateral Displacement

Similarly, the effect of the NWQD being laterally displaced is examined. In contrast to the NWQD tilt scenario, here the NWQD is completely off axis without inducing any angle, as depicted in Figure 9 (b) (inset image). Therefore, if the emitted light cone is laterally misplaced, it will result in the point of intersection with the microsphere's surface occurring a few nanometers away from its center. This will lead the photonic nanojet to be formed with no axial symmetry related to microsphere's - waveguide axis, pointing now with an angle depending on the axis misalignment of the NWQD, as shown in Figure 9.
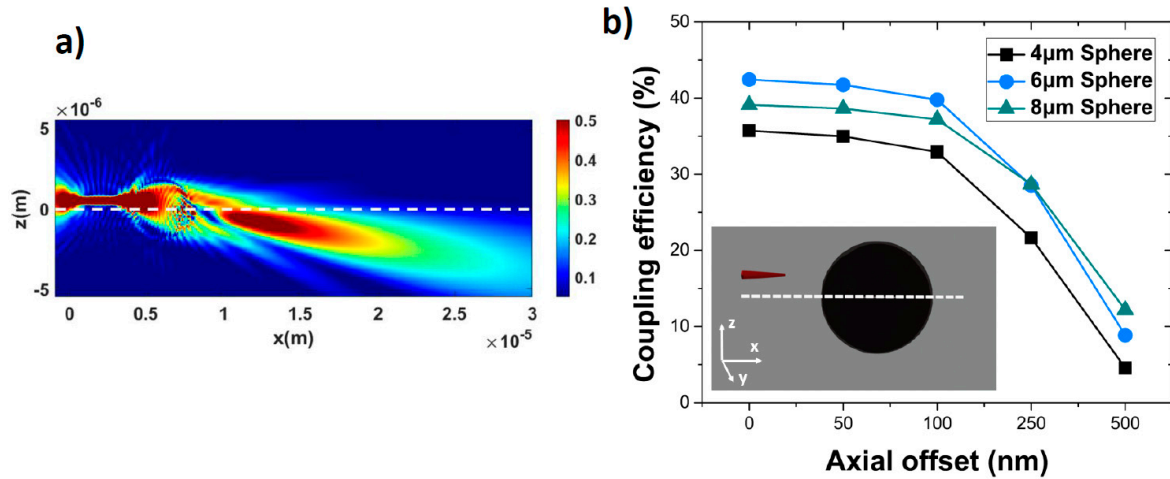
Figure 9. a) Photonic nanojet formed through a 4 μm microsphere with the NQD placed 500 nm away from the center of the microsphere in the Z- direction. b) NWQD-WG coupling values as a function of the axial misalignment. Inset image illustrates the axial offset of the nanowire.

In Figure 9 (b), the coupling efficiency values are extracted for a NWQD – microsphere – waveguide arrangement where the NQD is laterally in Z-axis (or in the symmetric Y-axis) by 50, 100, 250 and 500 nanometers, for 4, 6 and 8 μm diameter microspheres. It is evident that for an offset up to 100 nm the coupling efficiency for all cases is decreased by just ~2%. By moving the NWQD further away, though, the coupling efficiency starts to decrease at a higher rate, leading to an output value of ~10% at 500 nm off. Also, as expected, the larger 8 μm microsphere appears to be more tolerant since the displacement for smaller spheres will shift the NWQD emission even further from the center of the microsphere.

4.4. Effect of Sphericity Ratio

The efficiency of the proposed coupling scheme is also examined in terms of the microsphere shape. Chemically produced microspheres, typically, have a high sphericity ratio approaching the perfect spherical shape. However, there is a small percentage of microparticles that are not perfect spheres, rather have a more elliptical shape.

FDTD simulations were performed for the case of a microsphere (n = 1.9, 6 μm diameter) between the NWQD and the waveguide which is elongated in either the Y-axis (or equivalently the Z-axis due to symmetry) or the X-axis, while the propagation of light is monitored in the X-axis. The ellipticity of the microsphere (or ellipsoid percentage) is defined here as e = (a-b)/b, where a and b are the sphere radii in Y(Z) and X main axes. It is shown that the effect of the ellipsoidal microsphere medium results in linear decrease of the coupling efficiency as the sphere deformation and ellipsoid percentage increases. The coupling efficiency values are presented in Figure 10 (a) for both X-axis and Y-axis, and in Figure 10 (b) the electric field distribution along the X propagation axis is presented for a number of ellipsoids prolonged in the both axes at a percentage of up to 20%. It is observed an anomalous behavior for the Y elongation case as for a small deformation of 5% it seems that the coupling is increased which could be attributed to the specific more efficient collection of NWQD light by the microsphere's increased illuminated surface.
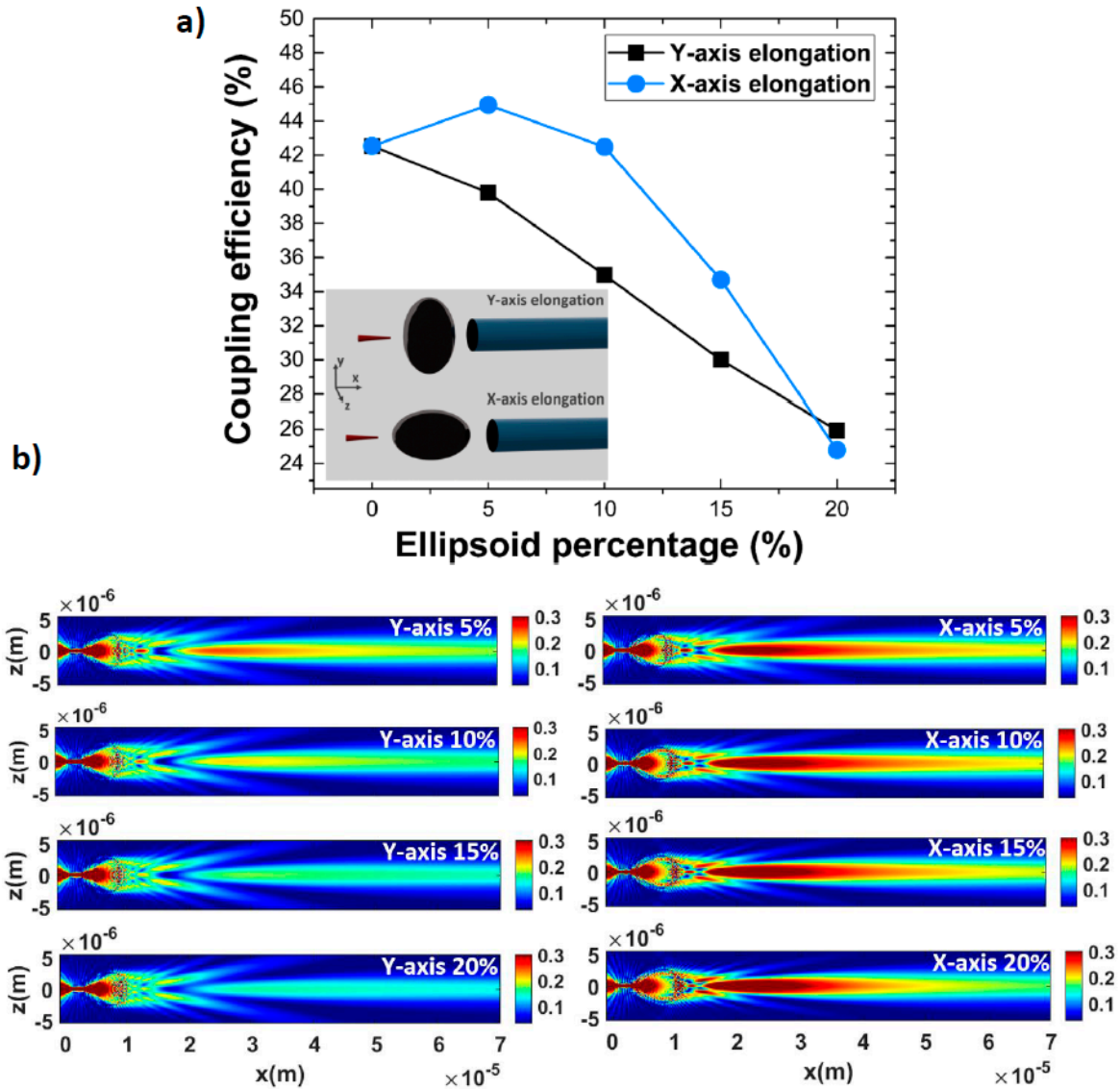
Figure 10. a) Coupling efficiency values for n = 1.9 microsphere at an increasing ellipsoid percentage from 0% to 20% in both Y-axis and X-axis and, b) corresponding electric field distributions along the XZ plane for Y-axis and X-axis elongated ellipsoids.

4.5. Effect of Operating Wavelength

Finally, in the showcased results we considered a NWQD emitter centered at 880 nm, however, in practical PICs one or more single photon sources can be incorporated emitting in more than one wavelength. Therefore, the robustness of the proposed configuration needs to be examined for different emission wavelengths other than the optimal designed one. The requirement is that a specific microsphere can couple light from different NWQDs emitted at different adjacent wavelengths, easing thus the hybrid circuit fabrication by using only one type and size of microsphere at different/multiple input ports. Furthermore, new developments in NWQDs have enabled the integration of multiple QDs in a single nanowire [50] and therefore a single optimized microsphere should ideally couple light efficiently at the multiple wavelengths corresponding to multiple QDs in a nanowire. With the considered nanowire we examine its operation with three different QDs operating and emitting at 880 nm, 910 nm, and 940 nm wavelengths. The QD emission, simulated by a dipole moment incorporated in the nanowire.

As can be seen in Figure 11 the dipole emission exhibits a coupling efficiency to the specific nanowire waveguide of ~70% for 880 nm wavelength, dropping to ~60% for 910 nm and to ~50% for

940 nm wavelengths. In Figure 11 is presented also the total coupling performance from nanowire to the waveguide by considering a coupling scheme with a 6 μm diameter microsphere of n = 1.9. Inspecting this decreasing trend in both coupling curves in Figure 11, as the wavelength increases, it indicates that the lower overall coupling values in the longer wavelengths is due to the initial coupling of the QD to the nanowire's waveguide structure for increased wavelength values, denoting that the coupling through the microsphere is not greatly affected by different wavelengths. Therefore, a hybrid circuit with an embedded specific microsphere can be operable for a range of wavelengths without complicating the structure, and by allowing also nanowire with multiple quantum dots. The simultaneous action of multi dots in a nanowire, coupled through a single microsphere could enable the efficient also multiwavelength operation in such hybrid circuits.
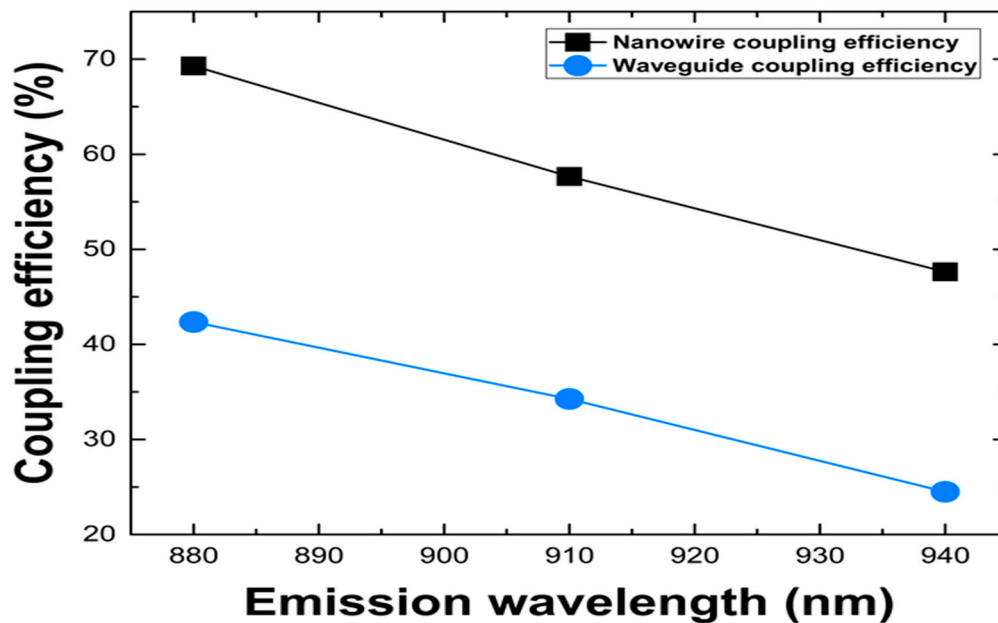

Figure 11. Coupling efficiency values in the nanowire itself and in the channel waveguide for QDs emission centered at 880, 910, and 940 nm wavelengths.

4. Conclusions

The paper deals with current challenges in the integration of single photon sources in optical waveguides for the development of hybrid quantum optical circuits and devices for quantum manipulation and processing of single photons towards quantum computing, communications and sensing applications. One major category of single photon sources is based on quantum dots that are embedded in semiconductor optical nanowires (NWQD). A recently published study [43] identified in a systematic way the serious limitations for coupling NWQD in low refractive index contrast channel waveguides, which are usually fabricated in Silica based platform by lithography or by direct Laser writing, or also generally by in-diffusion processes in various material platforms, thus limiting the coupling efficiency to <5% which is impractical for quantum applications.

This study proposed for the first time a method for the efficient light coupling of semiconductor nanowires to optical waveguides, by the introduction between them of a dielectric microsphere suitably designed, in terms of: 1) Size of the microsphere, 2) Refractive index of microsphere, 3) Distance between the nanowire and the microsphere, 4) Distance between microsphere and waveguide. Such an optimal arrangement assures the generation of a photonic nanojet from the illuminated microsphere with suitable spatial and optical characteristics that enable the efficient excitation of waveguide's eigenmodes and finally the light coupling to the channel waveguide through the microsphere.

The proposed method is demonstrated in the case of a typical InP nanowire with an embedded InAsP quantum dot, emitting at 880 nm, with 4 μm length and 200 nm diameter. The considered waveguide simulated a silica based cylindrical waveguide with 3μm diameter and refractive index raise of $5 \cdot 10^{-3}$ compared to pure silica, attributed to typical Laser induced refractive index change. It was demonstrated that by using readily available microspheres of Barium Titanate (n=1.9) or Alumina (n=1.76) with diameters around 5 μm it could be achieved coupling > 45%, while for achievable Laser written waveguides with refractive index difference > $5 \cdot 10^{-3}$ the coupling could easily exceed 50%. By properly incorporating Bragg gratings as reflectors to the back propagating light of nanowire this coupling could be enhanced even further. The study showed also that the tolerances in terms of the NWQD, microsphere, and waveguide relative positioning and misalignment can be perfectly satisfied by the state-of-the-art micromanipulation capabilities and therefore the standardization of the process could provide a robust and viable solution.

The above findings offer new opportunities towards the realization of silica based hybrid integrated photonic circuits, with on-chip integration of multiple nanowire single photon emitters with application especially in the most challenging case of directly Laser written waveguides of low refractive index contrast in silica and silica-on-silicon platform.

The current study seeks to demonstrate the successful coupling of NWQD to low confinement waveguides through realizable approaches in specific cases, while due to the complication of the study cannot provide at this stage generic engineering rules for designing and selecting the appropriate microspheres, although this theoretical study based on analytical formulation as in [48] could be triggered by this work. Further work of the fabrication tolerances and integration approaches in specific Silica on Silicon platform is under consideration and will be reported in a future study.

It is strongly anticipated that the proposed coupling scheme which solves a challenging problem, will enable the facilitation of Silica based optical circuits towrds the development of highly customizable and scalable quantum photonic integrated circuits, which are crucial for quantum computing applications.

Patents: C. Riziotis: "Light coupling between nanowire and optical waveguide by microsphere photonic nanojet," European Patent Office, Patent Application Number EP23386114.5 (Filing date 09-11-2023).

Supplementary Materials: The supplementary material section provides details of the coupling mechanism, for the coupling arrangement configurations presented in section 3.2 of the manuscript, for microspheres of refractive indices with values n = 1.6, 1.7, 1.76, 1.9, 2.0, 2.2, and 2.5, and with various diameters. For each individual graph in Figure 4 of the manuscript corresponding to a specific refractive index, the Figures S1 - S7 present visually the coupling mechanism by the photonic nanojet's excitation, for various examined microspheres' diameters, and for a specific distance L which corresponds to the maximum observed coupling value. Each one of the Figures S1(a) -S7(a) presents the light propagation along 120μm distance, and also in Figures S1(b) -S7(b) a magnified version of the graphs of Figure 5, for a greater propagation distance of 70μm. Figures S3(c), and S4(c) provide additionally, for comparison two indicative suboptimum coupling cases for comparison with the corresponding optimum cases.

Author Contributions: Conceptualization: C.R.; Methodology, C.R.; Validation, C.R., S.T., K.T., J.C.G., A.W.E. V.Z., P.G.R.S.; Formal Analysis, C.R., S.T., K.T.; Investigation, C.R., S.T., K.T., J.C.G., A.W.E. V.Z., P.G.R.S., C.R.; Writing – Original Draft Preparation, C.R., S.T., K.T., Writing – Review & Editing, C.R., S.T., K.T., J.C.G., A.W.E. V.Z., P.G.R.S.; Visualization, S.T., K.T.; Supervision, C.R., V.Z, P.G.R.S.; Project Administration, C.R.; Funding Acquisition, C.R.;

Conflicts of Interest: The authors declare no conflict of interest.

References

1. A. W. Elshaari, W. Pernice, K. Srinivasan, O. Benson, and V. Zwiller, "Hybrid integrated quantum photonic circuits," Nature Photonics, vol. 14, no. 5, 2020, pp. 285–298.
2. J. Wang, F. Sciarrino, A. Laing, and M. G. Thompson, "Integrated photonic quantum technologies," Nature Photonics, vol. 14, no. 5, 2019, pp. 273–284.
3. A. Politi, M. J. Cryan, J. G. Rarity, S. Yu, and J. L. O'Brien, "Silica-on-silicon waveguide quantum circuits," Science, vol. 320, no. 5876, 2008, pp. 646–649.
4. J. C. Matthews, A. Politi, A. Stefanov, and J. L. O'Brien, "Manipulation of multiphoton entanglement in waveguide quantum circuits," Nature Photonics, vol. 3, no. 6, 2009, pp. 346–350.
5. P. J. Shadbolt, M. R. Verde, A. Peruzzo, A. Politi, A. Laing, M. Lobino, J. C. Matthews, M. G. Thompson, and J. L. O'Brien, "Generating, manipulating and measuring entanglement and mixture with a reconfigurable photonic circuit," Nature Photonics, vol. 6, no. 1, 2011, pp. 45–49.
6. A. Laing, A. Peruzzo, A. Politi, M. R. Verde, M. Halder, T. C. Ralph, M. G. Thompson, and J. L. O'Brien, "High-fidelity operation of quantum photonic circuits," Applied Physics Letters, vol. 97, no. 21, 2010, p. 211109.
7. B. J. Smith, D. Kundys, N. Thomas-Peter, P. G. R. Smith, and I. A. Walmsley, "Phase-controlled integrated photonic quantum circuits," Optics Express, vol. 17, no. 16, 2009, p. 13516.
8. G. Corrielli, A. Crespi, R. Geremia, R. Ramponi, L. Sansoni, A. Santinelli, P. Mataloni, F. Sciarrino, and R. Osellame, "Rotated waveplates in integrated waveguide optics," Nature Communications, vol. 5, no. 1, 2014, p.4249.
9. L. Sansoni, F. Sciarrino, G. Vallone, P. Mataloni, A. Crespi, R. Ramponi, and R. Osellame, "Polarization entangled state measurement on a chip," Physical Review Letters, vol. 105, no. 20, 2010, p.200503.
10. A. Crespi, R. Ramponi, R. Osellame, L. Sansoni, I. Bongioanni, F. Sciarrino, G. Vallone, and P. Mataloni, "Integrated photonic quantum gates for polarization qubits," Nature Communications, vol. 2, no. 1, 2011, p. 566.
11. A. Aspuru-Guzik and P. Walther, "Photonic quantum simulators," Nature Physics, vol. 8, no. 4, 2012, pp. 285–291.
12. A. Peruzzo, J. McClean, P. Shadbolt, M.-H. Yung, X.-Q. Zhou, P. J. Love, A. Aspuru-Guzik, and J. L. O'Brien, "A variational eigenvalue solver on a photonic quantum processor," Nature Communications, vol. 5, no. 1, 2014, p.4213.
13. J. M. Arrazola, T. R. Bromley, J. Izaac, C. R. Myers, K. Brádler, and N. Killoran, "Machine learning method for state preparation and gate synthesis on photonic quantum computers," Quantum Science and Technology, vol. 4, no. 2, 2019, p. 024004.
14. A. Peruzzo, P. Shadbolt, N. Brunner, S. Popescu, and J. L. O'Brien, "A quantum delayed-choice experiment," Science, vol. 338, no. 6107, 2012, pp. 634–637.
15. J. Carolan, M. Mohseni, J. P. Olson, M. Prabhu, C. Chen, D. Bunandar, M. Y. Niu, N. C. Harris, F. N. Wong, M. Hochberg, S. Lloyd, and D. Englund, "Variational quantum unsampling on a quantum photonic processor," Nature Physics, vol. 16, no. 3, 2020, pp. 322–327.
16. C. Sparrow, E. Martín-López, N. Maraviglia, A. Neville, C. Harrold, J. Carolan, Y. N. Joglekar, T. Hashimoto, N. Matsuda, J. L. O'Brien, D. P. Tew, and A. Laing, "Simulating the vibrational quantum dynamics of molecules using photonics," Nature, vol. 557, no. 7707, 2018, pp. 660–667.
17. G. R. Steinbrecher, J. P. Olson, D. Englund, and J. Carolan, "Quantum Optical Neural Networks," npj Quantum Information, vol. 5, no. 1, 2019, p. 60.
18. N. Somaschi, V. Giesz, L. De Santis, J. C. Loredo, M. P. Almeida, G. Hornecker, S. L. Portalupi, T. Grange, C. Antón, J. Demory, C. Gómez, I. Sagnes, N. D. Lanzillotti-Kimura, A. Lemaître, A. Auffeves, A. G. White, L. Lanco, and P. Senellart, "Near-optimal single-photon sources in the solid state," Nature Photonics, vol. 10, no. 5, 2016, pp. 340–345.
19. X. Ding, Y. He, Z.-C. Duan, N. Gregersen, M.-C. Chen, S. Unsleber, S. Maier, C. Schneider, M. Kamp, S. Höfling, C.-Y. Lu, and J.-W. Pan, "On-demand single photons with high extraction efficiency and near-unity indistinguishability from a resonantly driven quantum dot in a micropillar," Physical Review Letters, vol. 116, no. 2, 2016, p. 020401.
20. A. Sipahigil, K. D. Jahnke, L. J. Rogers, T. Teraji, J. Isoya, A. S. Zibrov, F. Jelezko, and M. D. Lukin, "Indistinguishable photons from separated silicon-vacancy centers in Diamond," Physical Review Letters, vol. 113, no. 11, 2014,   p. 113602.
21. S. Bogdanov, M. Y. Shalaginov, A. Boltasseva, and V. M. Shalaev, "Material platforms for integrated quantum photonics," Optical Materials Express, vol. 7, no. 1, 2016, pp. 111-132.
22. B. Calkins, P. L. Mennea, A. E. Lita, B. J. Metcalf, W. S. Kolthammer, A. Lamas-Linares, J. B. Spring, P. C. Humphreys, R. P. Mirin, J. C. Gates, P. G. Smith, I. A. Walmsley, T. Gerrits, and S. W. Nam, "High quantum-

efficiency photon-number-resolving detector for photonic on-chip information processing," Optics Express, vol. 21, no. 19, 2013, pp. 22657-22670.

23. P. L. Mennea, W. R. Clements, D. H. Smith, J. C. Gates, B. J. Metcalf, R. H. Bannerman, R. Burgwal, J. J. Renema, W. S. Kolthammer, I. A. Walmsley, and P. G. R. Smith, "Modular linear optical circuits," Optica, vol. 5, no. 9, 2018, pp. 1087-1090.

24. Q.Zhang, M. Li, Y. Chen, X. Ren, R. Osellame, Q. Gong, and Y. Li, "Femtosecond laser direct writing of an integrated path-encoded CNOT quantum gate," Opt. Mater. Express, vol. 9, 2019, pp. 2318-2326.

25. S. Atzeni, A.S. Rab, G. Corrielli, E. Polino, M. Valeri, P. Mataloni, N. Spagnolo, A. Crespi, F. Sciarrino, and R. Osellame, "Integrated sources of entangled photons at the telecom wavelength in femtosecond-laser-written circuits," Optica, vol. 5, 2018, pp. 311-314.

26. P. Senellart, G. Solomon, and A. White, "High-performance semiconductor quantum-dot single-photon sources," Nature Nanotechnology, vol. 12, no. 11, 2017, pp. 1026–1039.

27. Y. Arakawa and M. J. Holmes, "Progress in quantum-dot single photon sources for quantum information technologies: a broad spectrum overview," Applied Physics Reviews, vol. 7, no. 2, 2020, p. 021309.

28. C.-Y. Lu and J.-W. Pan, "Quantum-dot single-photon sources for the quantum internet," Nature Nanotechnology, vol. 16, no. 12, 2021, pp. 1294–1296

29. J. Claudon, J. Bleuse, N. S. Malik, M. Bazin, P. Jaffrennou, N. Gregersen, C. Sauvan, P. Lalanne, and J.-M. Gérard, "A highly efficient single-photon source based on a quantum dot in a photonic nanowire," Nature Photonics, vol. 4, no. 3, 2010, pp. 174–177.

30. H. Mäntynen, N. Anttu, Z. Sun, and H. Lipsanen, "Single-photon sources with quantum dots in III–V nanowires," Nanophotonics, vol. 8, no. 5, 2019, pp. 747–769.

31. J. Chang, J. Gao, I. Esmaeil Zadeh, A.W. Elshaari, and V. Zwiller. "Nanowire-based integrated photonics for quantum information and quantum sensing" Nanophotonics, vol. 12, no. 3, 2023, pp. 339-358.

32. K. Mnaymneh, D. Dalacu, J. McKee, J. Lapointe, S. Haffouz, J. F. Weber, D. B. Northeast, P. J. Poole, G. C. Aers, and R. L. Williams, "On-chip integration of single photon sources via evanescent coupling of tapered nanowires to SiN waveguides," Advanced Quantum Technologies, vol. 3, no. 2, 2019, p. 1900021.

33. A. W. Elshaari, I. E. Zadeh, A. Fognini, M. E. Reimer, D. Dalacu, P. J. Poole, V. Zwiller, and K. D. Jöns, "On-chip single photon filtering and multiplexing in hybrid quantum photonic circuits," Nature Communications, vol. 8, no. 1, 2017, p. 379.

34. M. Davanco, J. Liu, L. Sapienza, C. Z. Zhang, J. V. De Miranda Cardoso, V. Verma, R. Mirin, S. W. Nam, L. Liu and K. Srinivasan, "Heterogeneous integration for on-chip quantum photonic circuits with single quantum dot devices," Nature Communications, vol. 8, 2017, p. 889.

35. I. E. Zadeh, A. W. Elshaari, K. D. Jöns, A. Fognini, D. Dalacu, P. J. Poole, M. E. Reimer, and V. Zwiller, "Deterministic integration of single photon sources in silicon based photonic circuits," Nano Letters, vol. 16, no. 4, 2016, pp. 2289–2294.

36. J.-H. Kim, S. Aghaeimeibodi, C. J. Richardson, R. P. Leavitt, D. Englund, and E. Waks, "Hybrid integration of solid-state quantum emitters on a silicon photonic chip," Nano Letters, vol. 17, no. 12, 2017, pp. 7394–7400.

37. L. Athanasekos, M. Vasileiadis, A. El Sachat, N.A. Vainos, and C. Riziotis, "ArF excimer laser microprocessing of polymer optical fibers for photonic sensor applications", Journal of Optics, vol. 17, 2015, p. 015402.

38. K. Kalli, C. Riziotis, A. Posporis, C. Markos, C. Koutsides, S. Ambran, A. S. Webb, C. Holmes, J. C. Gates, J. K. Sahu, and P. G. R. Smith, "Flat fibre and femtosecond laser technology as a novel photonic integration platform for optofluidic based biosensing devices and lab-on-chip applications: Current results and future perspectives," Sensors and Actuators B: Chemical, vol. 209, 2015, pp. 1030–1040.

39. G. Corrielli, A. Crespi, R. Osellame, "Femtosecond laser micromachining for integrated quantum photonics," Nanophotonics, vol. 10, no. 15, 2021, pp. 3789-3812.

40. G. D. Marshall, A. Politi, J. C. F. Matthews, P. Dekker, M. Ams, M. J. Withford, and J. L. O'Brien, "Laser written waveguide photonic quantum circuits," Opt. Express, vol. 17, no.15 2009, pp. 12546–12554.

41. I. J. Sparrow, P. G. Smith, G. D. Emmerson, S. P. Watts, and C. Riziotis, "Planar Bragg grating sensors—fabrication and applications: A Review," Journal of Sensors, vol. 2009, 2009, p. 607647.

42. S.I. Tsintzos, K. Tsimvrakidis, A. Sinani, A. Bogris, J.C. Gates, P.G.R. Smith, A.W. Elshaari, V. Zwiller, and C. Riziotis, "Design and fabrication challenges of integrated optical circuits for quantum computing applications", 21st International Conference on Transparent Optical Networks ICTON-2023, IEEE, Paper Mo.B6.4.

43. K. Tsimvrakidis, S.I. Tsintzos, J.C. Gates, P.G.R. Smith, A.W. Elshaari, V. Zwiller, and C. Riziotis, "Nanowire integration in silica based integrated optical circuits: limitations and challenges towards quantum computing," Optics & Laser Technology, vol. 170, 2024, p. 110276.

44. S.I. Tsintzos, K. Tsimvrakidis, A. Sinani, J.C. Gates, A.W. Elshaari, P.G.R. Smith, V. Zwiller, and C. Riziotis, "Enabling light coupling between nanowires and low refractive index contrast optical waveguides towards

scalable quantum circuits", SPIE PHOTONICS WEST 2024. Conference OE201   Integrated Optics: Devices, Materials, and Technologies XXVIII. 29 January - 1 February 2024, San Francisco, CA, USA.

45. D. Dalacu, K. Mnaymneh, J. Lapointe, X. Wu, P. J. Poole, G. Bulgarini, V. Zwiller, and M. E. Reimer, "Ultraclean emission from InAsP quantum dots in defect-free wurtzite InP nanowires," Nano Letters, vol. 12, no. 11, 2012, pp. 5919–5923.

46. A. Darafsheh, "Photonic nanojets and their applications," Journal of Physics: Photonics, vol. 3, no. 2, 2021, p. 022001.

47. Z. Chen, A. Taflove, and V. Backman," Photonic nanojet enhancement of backscattering of light by nanoparticles: a potential novel visible-light ultramicroscopy technique," Optics Express, vol. 12, no. 7, 2004, pp. 1214-1220.

48. G. Gouesbet, G. Grehan, and B. Maheu, "Scattering of a Gaussian beam by a Mie scatter center using a Bromwich formalism," Journal of Optics, vol.16, no. 2, 1985, pp. 83-93.

49. J. Zhu and L. L. Goddard, "Spatial control of photonic nanojets," Optics Express, vol. 24, no. 26, 2016 pp. 30444-30464.

50. P. Laferrière, E. Yeung, L. Giner, S. Haffouz, J. Lapointe, G. C. Aers, P. J. Poole, R. L. Williams, and D. Dalacu, "Multiplexed single-photon source based on multiple quantum dots embedded within a single nanowire," Nano Letters, vol. 20, no. 5, 2020, pp. 3688-3693.